



1 **Hazard assessment modeling and software development of**
2 **earthquake-triggered landslides in the Sichuan-Yunnan area, China**

3 Xiaoyi Shao^{1,2}, Siyuan Ma^{3,4}, Chong Xu^{1,2*}

4 1. National Institute of Natural Hazards, Ministry of Emergency Management of China,

5 Beijing 100085, China

6 2. Key Laboratory of Compound and Chained Natural Hazards Dynamics, Ministry of

7 Emergency Management of China, Beijing 100085, China

8 3. Institute of Geology, China Earthquake Administration, Beijing, 100029, China;

9 4. Key Laboratory of Seismic and Volcanic Hazards, Institute of Geology, China Earthquake

10 Administration, Beijing, 100029, China

11 *Corresponding to Chong Xu (xc11111111@126.com)

12 Abstract: To enhance the timeliness and accuracy of spatial prediction of co-
13 seismic landslides, we propose an improved three-stage spatial prediction strategy and
14 developed a corresponding hazard assessment software named Mat.LShazard V1.0.
15 Based on this software, we evaluate the applicability of this improved spatial
16 prediction strategy in six earthquake events that have occurred near the Sichuan
17 Yunnan region including the Wenchuan, Ludian, Lushan, Jiuzhaigou, Minxian and
18 Yushu earthquakes. The results indicate that in the first stage (within a half-hour of the
19 earthquake), except for the 2013 Minxian earthquake, the AUC values of the modelling
20 performance in other five events are above 0.8. Among them, the AUC value of the
21 Wenchuan earthquake is the highest, reaching 0.947. The prediction results in the first
22 stage can meet the requirements of emergency rescue with immediately obtaining the
23 overall predicted information of the possible coseismic landslide locations in the
24 quake-affected area. In the second and third stages (Within 12 hours of the quake),
25 with the improvement of landslide data quality, the prediction ability of the model
26 based on the entire landslide database is gradually improved. Based on the entire



27 landslide database, the AUC value of the six events exceeds 0.9, indicating a very high
28 prediction accuracy. Whether in the second or third stage (After 3 days of the seismic
29 event), the predicted landslide area (A_p) is in good agreement with the observed
30 landslide area (A_o). However, based on incomplete landslide data in the meizoseismal
31 area, A_p is much smaller than A_o . When the prediction model based on complete
32 landslide data is built, A_p is nearly identical to A_o . This study provides a new
33 application tool for coseismic landslide disaster prevention and mitigation in different
34 stages of emergency rescue, temporary resettlement, and later reconstruction after a
35 major earthquake.

36 Keywords: Major earthquake; Earthquake-induced landslide; Hazard assessment;
37 Logistic Regression model; Sichuan-Yunnan area;

38 **1 Introduction**

39 Coseismic landslides are one of the most widespread and destructive hazards
40 triggered by earthquakes in mountainous geological environments ([Robinson et al.,](#)
41 [2017](#)). The Sichuan Yunnan region of China has experienced frequent seismic activity
42 due to the characteristics of crustal movement and the action of active faults ([Cheng](#)
43 [et al., 2020](#); [Xu et al., 2005](#)). Furthermore, due to the unique subtropical monsoon
44 climate with rich and concentrated rainfall, the region is considered an intense
45 coseismic-landslide-prone zone ([Cui et al., 2009](#)). Therefore, scientific understandings
46 of the spatial distribution of earthquake-induced landslides in this area, followed by
47 near real-time emergency assessment ([Cao et al., 2019](#); [Tanyas et al., 2019](#)) and
48 medium and long-term risk assessment ([Guzzetti et al., 2005](#); [Lari et al., 2014](#)) can
49 effectively reduce the landslide risk after the earthquake, and also serve for emergency
50 rescue and town planning ([Lan et al., 2022](#)).

51 Evaluation and production of landslide susceptibility mapping can be broadly
52 categorized in three different types, including exploratory analysis based on
53 professional experience, Newmark model based on seismic landslide occurrence
54 mechanism, and the data driven-based machine learning model ([Shao and Xu, 2022](#);
55 [Tian et al., 2020](#)). In the application of expert knowledge, this method is heavily



56 influenced by subjective human factors, so human experience error is unavoidable.
57 The physical-based Newmark model is widely used in seismic landslide hazard
58 assessment of multiple earthquake events, including the 1994 Northridge, California,
59 earthquake ([Jibson et al., 2000](#)), the 2008 Wenchuan earthquake ([Ma and Xu, 2019a](#)),
60 and the 2017 Jiuzhaigou earthquake ([Liu et al., 2017](#)). However, since the simplified
61 Newmark method generalizes calculation process and the input parameters of the
62 evaluation results, the regional evaluation results are not ideal in earthquake
63 emergency assessment ([Liu et al., 2017](#); [Ma and Xu, 2019b](#)). In contrast, the data-
64 driven machine learning method is frequently employed and has the widest potential
65 for application, such as the Information Value Method ([Demir et al., 2013](#)), logistic
66 regression([Bai et al., 2015](#); [Dai et al., 2001](#); [Umar et al., 2014](#)), fuzzy logic([Ercanoglu](#)
67 [and Temiz, 2011](#); [Kritikos et al., 2015](#)), artificial neural network([Pradhan and Saro,](#)
68 [2010](#)), support vector machine([Xu et al., 2012](#); [Yao et al., 2008](#)). Among them, the LR
69 model is one of the most widely used models in the earthquake-induced landslides
70 susceptibility assessment by virtue of its simplicity, high efficiency, and high prediction
71 accuracy ([Reichenbach et al., 2018](#); [Shao and Xu, 2022](#)).

72 For a single earthquake event, rapidly identifying the high hazard area of
73 landslides is crucial for understanding the total earthquake impacts([Nowicki Jessee et](#)
74 [al., 2018](#); [Tanyas et al., 2019](#)). However, the issue of the data-driven machine learning
75 method is that the training model often needs detailed coseismic landslide data.
76 However, seismic landslide mapping is a difficult and time-consuming task, hindered
77 by issues relating to the collection and processing of appropriate satellite or aerial
78 images, cloud cover, and the slow speeds associated with manual identification and
79 mapping of large numbers of landslides([Robinson et al., 2017](#)). Consequently, the
80 evaluation result based on traditional methods lags behind practical emergency
81 response, and thus is unable to serve the short-term disaster prevention and
82 mitigation ([He et al., 2021](#); [Nowicki et al., 2014](#)).

83 To address the issue that the current spatial prediction of coseismic landslides is
84 not timely enough for practical application, [Ma et al. \(2020\)](#) propose a three-stage
85 spatial prediction strategy for seismic landslides, including emergency response (3



86 days after a major shock), temporary resettlement (3-60 days after the quake), and
87 late reconstruction (after 60 days), and use this strategy in the 2013 Lushan
88 earthquake event. In the emergency response stage, the Newmark model is used to
89 carry out rapid emergency hazard mapping in the several hours after the earthquake.
90 However, it should be noted that the Newmark model's prediction results are strongly
91 influenced by the input parameters ([Dreyfus et al., 2013](#)), and obtaining relatively
92 reasonable geotechnical parameters for a large area is extremely difficult ([Wang et al.,
93 2016](#); [Zhuang et al., 2019](#)). As a result, the accuracy of prediction results based on the
94 Newmark model is relatively low, and it cannot meet the needs of emergency
95 assessment ([Ma and Xu, 2019b](#)). At the same time, the three-stage prediction strategy
96 has only been tested in the Lushan earthquake, and its applicability in other seismic
97 events with different magnitudes and structural landform environments is still
98 required to be determined.

99 In recent years, the near real-time coseismic landslide models have become a
100 powerful tool for fast estimates of ground failure hazards. The core of these models is
101 to incorporate the hazard estimate from seismic events by including the ShakeMap
102 data for each earthquake (available in near real-time from the USGS), combined with
103 environmental factor data, thus allowing the model to be applied in near real-time for
104 future events. For example, [Nowicki et al. \(2014\)](#) combine shaking estimates with
105 proxies for slope, geology, and wetness with 1 km resolution to develop a globally
106 applicable model for near real-time prediction of coseismic landslides based on four
107 landslide inventories. Subsequently, [Nowicki Jessee et al. \(2018\)](#) expand the
108 observational landslide data set which includes 23 landslide inventories and develop a
109 new global empirical model. [Tanyas et al. \(2019\)](#) use 25 earthquake-induced landslides
110 and seven independent thematic variables based on logistic regression model to
111 establish a global slope unit-based model for the near real-time prediction of
112 earthquake-induced landslides. [Allstadt et al. \(2018\)](#) select the 2016 Mw 7.8 New
113 Zealand earthquake as a test case for evaluating the performance and near-real-time
114 response applicability of three published global earthquake-induced landslide models,
115 and the assessment results show that the global models have great potential in



116 earthquake landslide emergency assessment. Simultaneously, [Xu et al. \(2019\)](#) propose
117 a real probability prediction method of coseismic landslides utilizing the Bayesian
118 probability method and LR model, and establish a new generation of Chinese
119 earthquake-triggered landslide hazard model based on 9 real earthquake-triggered
120 landslide cases. However, the nationwide model's applicability in various earthquake
121 cases with different tectonic and geomorphologic environments needs to be further
122 tested.

123 In view of the issues encountered during the emergency assessment stage of the
124 three-stage spatial prediction strategy for coseismic landslides, the aim of this study is
125 to propose an improved three-stage spatial prediction strategy and develop a
126 corresponding Hazard assessment software called Mat.LShazard V1.0. Then, based on
127 this software, we evaluate the applicability of this improved spatial prediction strategy
128 in six earthquake events that have occurred near the Sichuan Yunnan region with
129 different tectonic and geomorphologic environments, including the 2008 Mw 7.9
130 Wenchuan earthquake, the 2014 Mw 6.6 Ludian earthquake, the 2013 Mw 6.6 Lushan
131 earthquake, the 2017 Mw 6.5 Jiuzhaigou earthquake, the 2013 Mw 5.9 Minxian
132 earthquake and the 2010 Mw 6.9 Yushu earthquake. The results of this study are
133 expected to provide technical supports for the emergency assessment and mid- and
134 long-term risk zoning of coseismic Landslides in Sichuan and Yunnan regions.

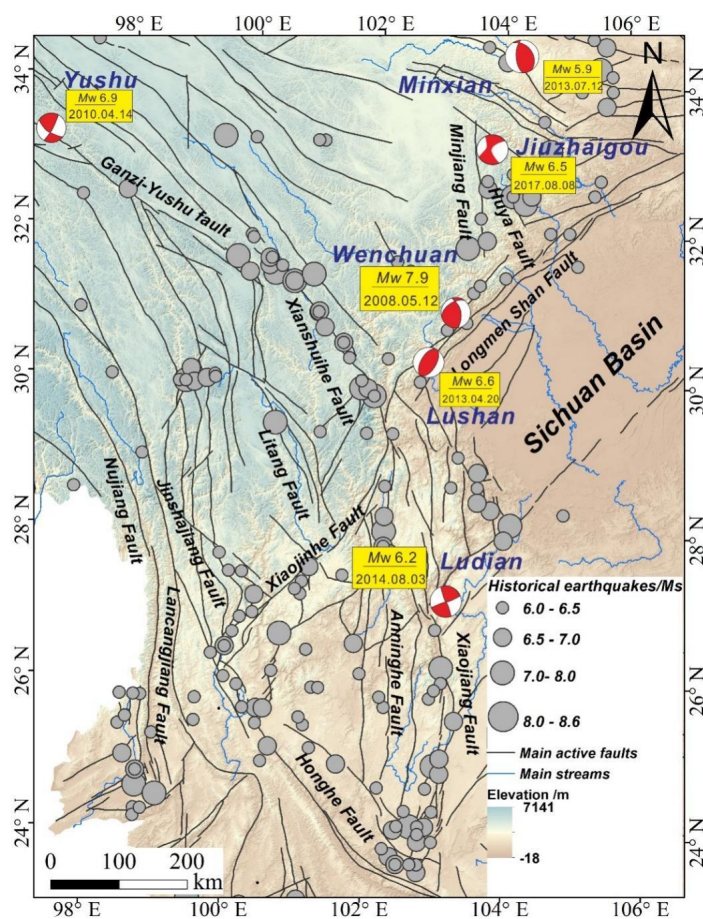
135 **2 Study area**

136 **2.1 Geological setting**

137 The Sichuan-Yunnan region is located on the eastern edge of the Tibetan Plateau.
138 Because of the Sichuan Basin blocking and the impact of fluid movement in the lower
139 crust, tectonic activities in this region are extremely complex ([Jiang et al., 2012](#);
140 [Tapponnier et al., 2001](#); [Zhang et al., 2003](#)). Furthermore, due to the intricate tectonic
141 mechanism, various types of active faults are developed, such as the Lancangjiang fault,
142 the Jinshajiang fault, the Xianshuihe fault, the Longmenshan fault, the Anninghe fault,
143 the Honghe fault, the Xiaojiang Fault, and other fault zones, which control the



144 occurrence of strong earthquakes in this area ([Cheng et al., 2020](#); [Ren et al., 2022](#); [Xu](#)
145 [et al., 2005](#)). The result shows that at least 16 magnitude 7.0 or stronger earthquake
146 events have occurred since 1327, including four earthquakes with magnitude larger
147 than 8.0. As a result, this area has also become the most severely affected region
148 associated with earthquake-induced landslide disasters ([Huang and Fan, 2013](#); [Zhao et](#)
149 [al., 2021](#)). Since 2008, multiple strong earthquakes have frequently struck this area,
150 which triggered massive coseismic landslides. For example, the 2008 Wenchuan
151 earthquake killed tens of thousands of people, with landslides accounting for 30% of
152 the total loss from the earthquake ([Cui et al., 2009](#)). The 2013 Lushan earthquake killed
153 196 people, with 24 missing, at least 11826 injured and more than 968 seriously injured
154 ([Xu et al., 2013](#)). These earthquake events induced a large number of coseismic
155 landslides, which not only seriously threatened the safety of people's lives and
156 property and traffic arteries, but also seriously affected the construction and operation
157 of Sichuan Tibet railway, Yunnan Tibet railway, hydropower resources development
158 and other major national projects.



159

160 Fig.1 Map showing the topography, earthquakes and tectonic setting of the Sichuan-Yunnan region

161 2.2 Six landslide inventories

162 Six landslide-triggering earthquakes have been investigated to test our model (Fig.
163 2). For all the available inventories, landslides have been mapped as polygons from
164 aerial photographs and satellite imagery, and also through field surveys (the 2008 Mw
165 7.9 Wenchuan earthquake ([Xu et al., 2014b](#)), the 2014 Mw 6.6 Ludian earthquake ([Wu
166 et al., 2020](#)), the 2013 Mw 6.6 Lushan earthquake ([Xu et al., 2015](#)), the 2017 Mw 6.5
167 Jiuzhaigou earthquake ([Tian et al., 2019](#)), the 2013 Mw 5.9 Minxian earthquake ([Tian
168 et al., 2016](#); [Xu et al., 2014a](#)), the 2010 Mw 6.9 Yushu earthquake ([Xu and Xu, 2014](#))).
169 Landslides in these inventories are reported without differentiating landslide types.
170 These landslide inventories have the following characteristics: (1) All landslides are



171 mapped as polygons with clear boundary information; (2) All landslides are visually
172 interpreted based on high-resolution images (3) All landslides are delineated within
173 the whole earthquake affected area.

174 The 2008 Mw 7.9 Wenchuan earthquake is the result of sudden dislocation of the
175 Yingxiu Beichuan fault in Longmenshan fault zone ([Xu et al., 2009](#)). This earthquake
176 has ruptured two large thrust faults along the Longmenshan thrust belt and produced
177 a 240-km-long surface rupture zone along the Yingxiu-Beichuan fault and a 72-km-long
178 surface rupture zone along the Guanxian-Jiangyou fault. The earthquake has triggered
179 nearly 200 thousand landslides, covering an area of about 311880 km².

180 The Mw 6.6 Lushan earthquake occurred on April 14, 2013, which is another
181 strong earthquake that occurred in the southwest section of the Longmenshan
182 mountain range since the 2008 Wenchuan earthquake. The earthquake triggered
183 more than 22528 landslides, covering an area of about 234.4 km².

184 The Mw5.9 Minxian earthquake on July 12, 2013 occurred within the Lintan-
185 Dangchang fault, located between the East Kunlun fault and the Northern margin of
186 the West Qinling fault ([Zheng et al., 2013](#)). The focal depth of this earthquake is 8.2
187 km. The earthquake triggered more than 6479 landslides, covering an area of about
188 830.2 km².

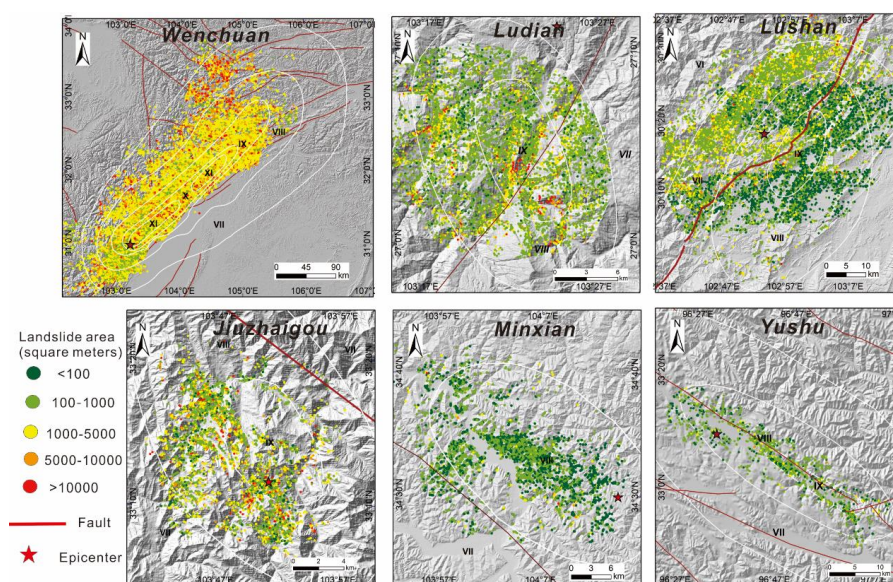
189 The seismogenic structure of the Mw 6.6 Ludian earthquake is the NNW-striking
190 Baogunao-Xiaohe fault between the Lianfeng fault and the Zhaotong Lianfeng fault.
191 The hypocentre is located at a depth of 12 km. The earthquake triggered more than
192 1024 landslides, covering an area of about 234.4 km².

193 The Mw 6.5 Jiuzhaigou earthquake occurred on 8 August 2017 in Sichuan
194 province, China. The depth of the hypocentre was estimated to be around 9 km. The
195 main seismogenic structure of this earthquake may be a branch of the tazang fault, or
196 the northern part of the Huya fault. According to the focal mechanism solution, the
197 strike of the seismogenic fault is NW-SE and the dip is SW; the fault is a left-lateral
198 strike-slip earthquake([Sun et al., 2018](#)). The earthquake triggered about 5986
199 landslides, and the total area is about 9.6km².

200 The Mw6. 9 Yushu earthquake occurred near Qinghai province on 4 April 2010.



201 The hypocenter is located at a depth of 17 km within the Ganzi–Yushu strike-slip
202 fault(Chen *et al.*, 2010). The earthquake produced a surface fracture zone with a strike
203 of about 300 ° and a length of 65km. The surface rupture zone is characterized by left-
204 lateral strike-slip fault. The surface rupture zone is composed of a series of extrusion
205 bulge and tension fractures (Chen *et al.*, 2010). The earthquake triggered almost 2036
206 landslides with an area of about 1455.3 km².



207
208 Fig.2 Six earthquake-induced landslide inventories used in this study. White lines show spatial
209 distribution of the seismic intensity, provided by the China Earthquake Networks Center(CENC)

210 3 Data and Software

211 3.1 Data sources

212 Seismic landslides are mainly controlled by earthquakes, topography, geology,
213 hydrology and other factors (Nowicki Jessee *et al.*, 2018; Reichenbach *et al.*, 2018). In
214 this study, 11 influencing factors are selected to establish the LR model for the second
215 and third stages, including elevation, slope angle, slope aspect, topographic relief,
216 curvature, topographic wetness index (TWI), vegetation coverage percentage, distance
217 from fault, lithology, annual average precipitation and seismic intensity.



218 The elevation data is from SRTM DEM, and its projection resolution is 30m ([Jarvis](#)
219 [et al., 2008](#)). The slope, aspect and curvature are extracted using this DEM and ArcGIS
220 software. Topographic relief and TWI are also computed using GRASS GIS based on this
221 DEM data. We consider a global data set that represents the maximum green
222 vegetation fraction (0–100%) to characterize the vegetation coverage of the land area
223 and the water bodies; the vegetation coverage is assigned as -1 ([Tateishi, 2010](#)). The
224 distribution of active fault data are acquired from National seismicity fault database
225 ([Xu et al., 2016](#)). The distance from the centroid of the grid cells to the nearest fault
226 are calculated using ArcGIS. The distribution of seismic intensity for every seismic
227 event is provided by China Earthquake Networks Center
228 (<https://www.cenc.ac.cn/cenc/zgdztw/index.html>), and then the raster format for the
229 seismic intensity is obtained by the Kriging interpolation.

230 The stratigraphic data are from the 1:2,500,000 geological map published by
231 China Geological Survey (<http://dcc.cgs.gov.cn/>). We divide the lithology into 12
232 categories according to the stratigraphic ages, which are Quaternary (Q), Tertiary (R),
233 Cretaceous (K), Jurassic (J), Triassic (Tr), Permian (P), Carboniferous (C), Devonian (D),
234 Silurian (S), Ordovician (O), Cambrian (\in) and Precambrian (Pre \in). The annual
235 average rainfall data are obtained from 1 km spatial resolution climate surfaces for
236 global land areas of WorldClim 2 dataset ([Fick and Hijmans, 2017](#)). Finally, the spatial
237 distribution of the 11 influencing factors is converted into a raster format with a grid
238 cell size of 30 m.

239 3.2 Mat.LShazard V1.0 Software description

240 3.21 The computational framework

241 A number of tools for landslide susceptibility assessment are already available in
242 current studies, such as GIS-based LSAT toolbox ([Polat, 2021](#)), LAND-SE implemented
243 in R ([Rossi and Reichenbach, 2016](#)), r.landslide module based on GRASSGIS
244 ([Bragagnolo et al., 2020](#)), GeoFIS ([Osna et al., 2014](#)), and LSAT PM v1.0 ([Torizin et al.,](#)
245 [2022](#)), providing great convenience for us to conduct the regional landslide



246 susceptibility assessment. However, to our knowledge, there is no specialized software
247 for seismic landslide Hazard assessment, particularly in the various needs of different
248 stages after a major earthquake.

249 Based on MATLAB, we develop an earthquake-induced Hazard assessment
250 software named Mat.LShazard V1.0. This section describes the computational
251 framework and operation of the software. A flowchart describing the module is
252 presented in Fig.3. Data input, model training, and model validation are the three main
253 components of the software. Landslide data and the influencing factors of the study
254 area are used for the input data. These data are in TIFF grid layer format. We employ
255 the LR model for model training. We train the logistic regression model using the
256 aforementioned input data, and then produce the seismic landslide hazards map.
257 Finally, in order to assess and confirm the accuracy of the model's prediction outputs,
258 three indexes are chosen for the verification of receiver operating characteristics (ROC)
259 curve, the confusion matrix and the predicted landslide area (A_p).

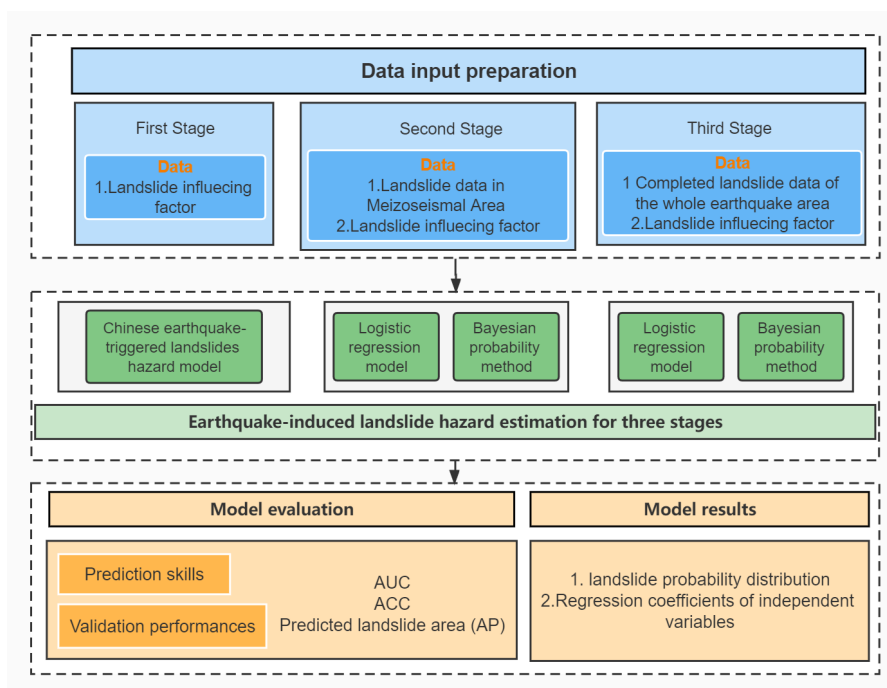
260 It is important to note that Mat.LShazard V1.0 is not the same as the traditional
261 landslide susceptibility software. The goal of this software is to meet the needs of
262 various stages following a major earthquake. As a result, for different stages, we
263 calculate seismic landslide hazard assessment results based on different LR models.
264 For the emergency rescue stage I ((Within a half-hour of the earthquake)), we select
265 the new generation of Chinese earthquake-triggered landslide hazard model, which is
266 established by 9 earthquake cases, including 306435 real earthquake landslide records
267 and 13 influencing factors with a 100m resolution ([Xu et al., 2019](#)). More detailed
268 theory and calculation procedures can be found in ([Xu et al., 2019](#)). In the absence of
269 seismic landslide data, this model can produce seismic landslide hazard distribution
270 map for stage I with only the seismic intensity map.

271 For temporary resettlement stage II (Within 12 hours of the quake), remote
272 sensing images can be gradually obtained following the earthquake. Based on visual
273 interpretation or automatic identification, we can obtain the seismic landslide
274 distribution map of the meizoseismal area, which can be used as the preliminary
275 results of this event. Combined with the influencing factors with 30m resolution and



276 incomplete landslide data, we can establish a new LR model and provide the seismic
277 landslide hazard distribution map for stage II.

278 For the late reconstruction stage III (3 days after the seismic event), a large
279 number of remote sensing images collected before and after the earthquake in the
280 quake-affected area can be obtained, which can effectively cover the entire
281 earthquake area, realizing the establishment of a comprehensive earthquake-induced
282 landslide inventory. At this stage, we combine the complete landslide data and
283 influencing factor data with 30m resolution to train and update the LR model, and
284 provide the seismic landslide hazard map for stage III.



285

286 Fig.3 Logical schema of the Mat.LShazard V1.0 software for earthquake-induced hazard assessment

287 3.22 Logistic Regression model

288 Logistic regression model (LR) is a statistical model that predicts the probability
289 of one event taking place by having the log-odds (the logarithm of the odds) for the
290 event be a linear combination of one or more independent variables ("predictors")



291 ([Dai and Lee, 2002](#); [Merghadi et al., 2020](#); [Tolles and Meurer, 2016](#)). It is a nonlinear
292 multivariate statistical model that has been widely used in landslide susceptibility
293 modeling ([Allstadt et al., 2018](#); [Broeckx et al., 2018](#); [Lin et al., 2017](#); [Massey et al.,](#)
294 [2018](#)). LR model converts dependent variables into binary logic variables that occur
295 (recorded as 1) and do not occur (recorded as 0). The relationship between landslide
296 occurrence probability and impact factors can be expressed as:

$$297 \quad Z = \beta_0 + \beta_1\chi_1 + \beta_2\chi_2 + \beta_3\chi_3 \dots \beta_i\chi_i \quad (1)$$

$$298 \quad P = 1/(1 + e^{-z}) \quad (2)$$

299 Where P represents the probability of landslide occurrence, ranging from 0 to 1.
300 Z represents the sum of linear weight values after variable superposition, χ_i denotes
301 each impact factor, β_i is the corresponding regression coefficient.

302 3.22 Bayesian probability method

303 The aim of this study is to develop a probability estimator for predicting the areal
304 extent of landslides. In other words, we correlate the resulting probability with spatial
305 extent (e.g., areas labeled 5% probability of landsliding contain about 5% landslides by
306 area). As a result, we generate sample points randomly in the study area. The points
307 within the landslide area are sliding samples, while the others are not; such setting
308 ensures that the ratio of sliding to non-sliding is equivalent to the probability of
309 coseismic landslides occurring in the study area. The coseismic landslide probability
310 (P_{cols}) in the region is simply defined as the ratio of the area of all landslides to the
311 total area of the region based on Bayesian theory:

$$312 \quad P_{cols} = \frac{A_l}{A_s} \times 100\% \quad (3)$$

313 where A_l is the total area of all coseismic landslides and A_s is the area of the entire
314 study area.

315 Based on the above Bayesian probability method and the corresponding landslide
316 surface data, we can randomly generate the corresponding landslide sample points
317 and non landslide sample points; thus, the predictive model can be constructed.



318 3.23 Model validation

319 In this study, three indexes including the receiver operating characteristics (ROC)
320 curve, the confusion matrix and the predicted landslide area (A_p) are used to evaluate
321 our results. First, we assess the modelling performance by checking the variation in
322 AUC value (varying between 0.5 for a random classification model and 1 for the best
323 performance), which is a metric referring to the area under the ROC Curve ([Brenning,](#)
324 [2005](#); [Swets, 1988](#)). Second, we use the confusion matrix for the performance
325 evaluations of the prediction results. The confusion matrix consists of four basic
326 characteristics (numbers) that are used to define the measurement metrics of the
327 classifier, which are TP (True Positive), TN (True Negative), FP (False Positive) and FN
328 (False Negative) ([Fawcett, 2006](#)), respectively. One of the most commonly used metrics
329 while performing classification is accuracy. The accuracy of a model through a
330 confusion matrix is calculated using the formula expressed as:

$$331 \text{ Accuracy} = \frac{TP + TN}{TN + FP + FN + TP} \quad (4)$$

332 Otherwise, in order to evaluate the model prediction performance, we also
333 calculate the predicted landslide area (A_p) of LR models based on A_p ([Allstadt et al.,](#)
334 [2018](#); [Shao et al., 2020b](#))

$$335 A_p = \sum_{i=1}^m \sum_{j=1}^n p_{i,j} A \quad (5)$$

336 in which $p_{i,j}$ is the probability of a landslide at pixel i and j , m is the number of
337 rows, n is the number of columns, and A is the pixel/cell area (constant).

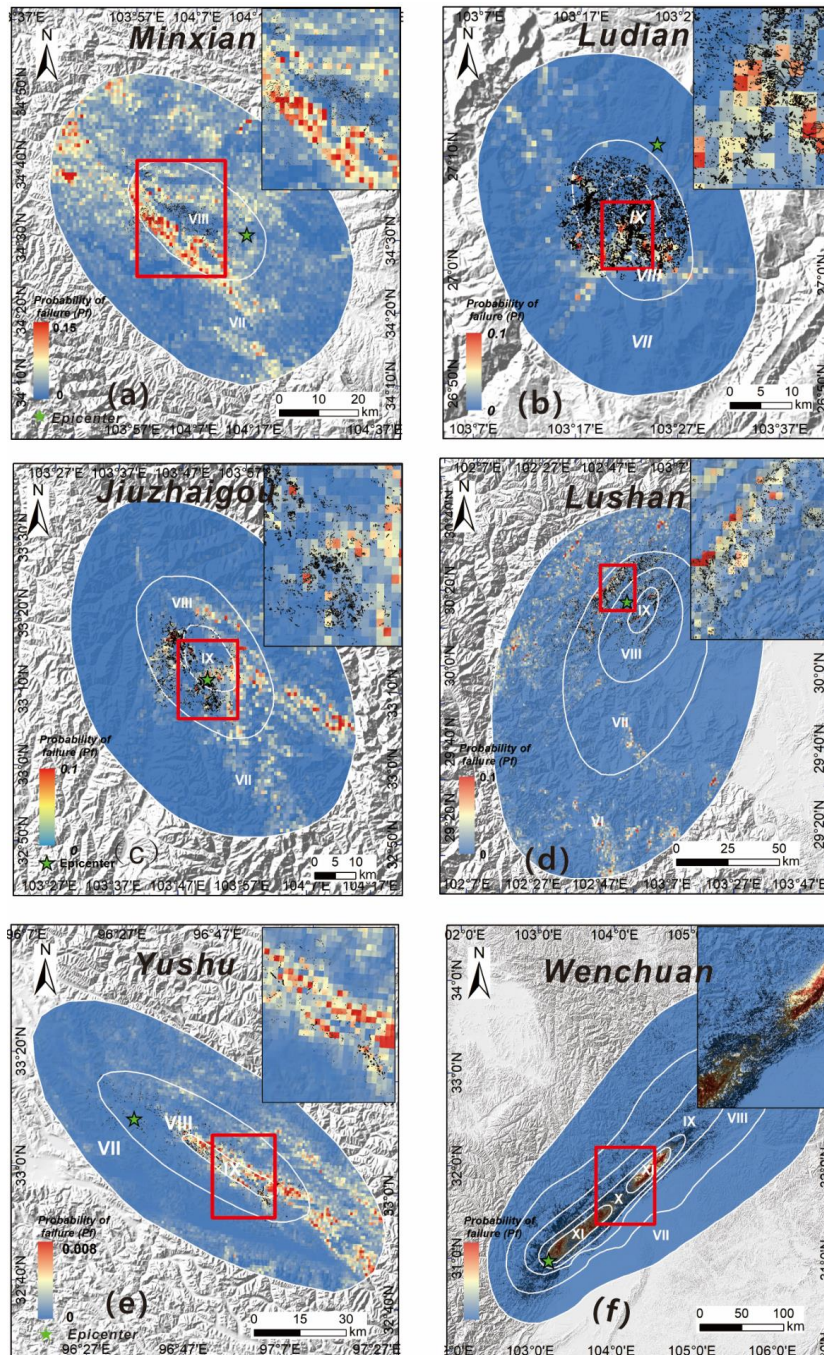
338 4 Results and analysis

339 4.1 First Stage

340 The landslide hazard estimate of six earthquake events in the first stage is
341 obtained using the Chinese earthquake-triggered landslide hazard model ([Xu et al.,](#)
342 [2019](#)). The predicted results in our software can be processed at the first stage by
343 entering the seismic intensity maps of six cases produced by CENC. Fig.4 shows the
344 predicted probability distribution for six earthquake events in the first stage. Overall,
345 the Chinese earthquake-triggered landslide hazard model has different forecasting



346 abilities for different earthquake events. For the Wenchuan earthquake, the prediction
347 results in this stage are reliable. The regions with high hazard risk are primarily found
348 in intensity X and XI, and the distribution of actual landslides also reveals that nearly
349 80% of the landslides are concentrated in the northeast area with intensity X and XI.
350 In addition, for the 2013 Lushan earthquake and the 2017 Jiuzhaigou earthquake, most
351 of the actual landslides are basically located in high-hazard-risk areas. Especially for
352 the Lushan earthquake, the prediction results can better forecast the northwest region
353 located in the epicenter region, which corresponds to the landslide-concentrated area.
354 For the 2010 Yushu earthquake, the high-hazard-risk area is located in the southeast
355 region with intensity VII and the whole region with intensity IX. The actual coseismic
356 landslides of the Yushu earthquake are primarily distributed in regions with intensity
357 IX, indicating that with the exception of the overestimated southeast region with
358 intensity VII, the remaining area can accurately predict the potential high susceptibility
359 areas. However, the prediction results of the 2013 Minxian earthquake are barely
360 satisfactory. According to Fig.4, the high-hazard-risk prediction areas are primarily
361 concentrated in the northwest region with intensity VII and the southwest region with
362 intensity VIII. However, according to the actual distribution of landslides, the most
363 landslides triggered by this earthquake are located in the central region with intensity
364 VIII. Namely, the prediction results do not accurately predict the actual landslide
365 distribution, and the majority of coseismic landslides occur in low-hazard-risk
366 prediction areas.



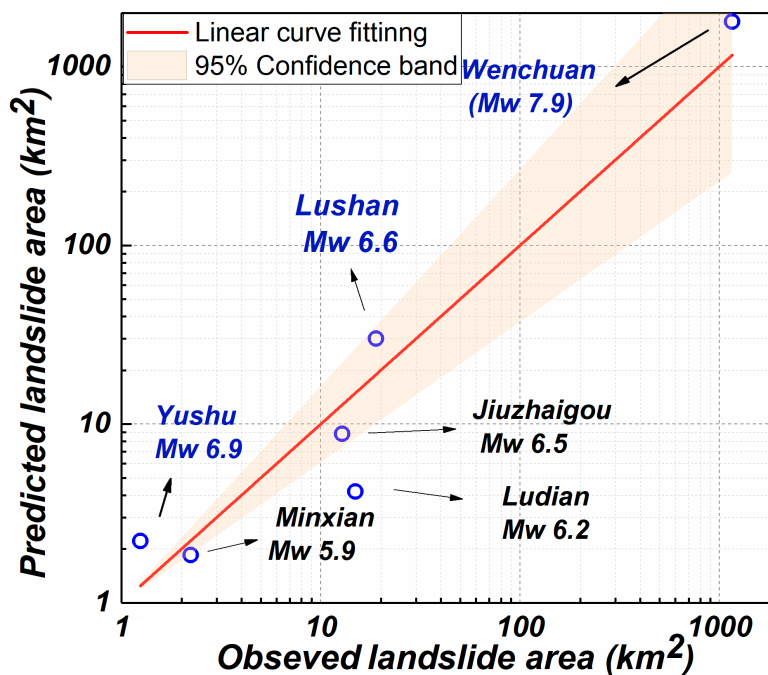
367

368 Fig.4 Maps showing predicted landslide probability distribution for six earthquake events in the
369 first stage; (a) the 2013 Mw 5.9 Minxian earthquake; (b) the 2014 Mw 6.6 Ludian earthquake; (c)



370 the 2017 Mw 6.5 Jiuzhaigou earthquake; (d) the 2013 Mw 6.6 Lushan earthquake; (e) the 2010 Mw
371 6.9 Yushu earthquake; (f) the 2008 Mw 7.9 Wenchuan earthquake.

372 We compare the predicted landslide area (A_p) in the first stage with the actual
373 landslide area. Fig.5 shows that the slope of the fitting curve between the predicted
374 and actual areas of the six earthquakes is close to one. The A_p for the Yushu, Lushan,
375 and Wenchuan earthquakes are on the high side, with an error range of 50%-78%. On
376 the other hand, the A_p of Minxian Ludian, and Jiuzhaigou earthquake, are on the low
377 side, with an error range of 17%-30%. In general, the prediction results meet the
378 requirements of emergency rescue with quickly obtaining the predicted information
379 of the possible coseismic landslide locations in the whole quake-affected area.



380
381 Fig.5 Relationships between the observed landslide area (A_o) and the predicted landslide area (A_p)

382 for six earthquake events in the first stage.

383 4.2 Second and Third Stages

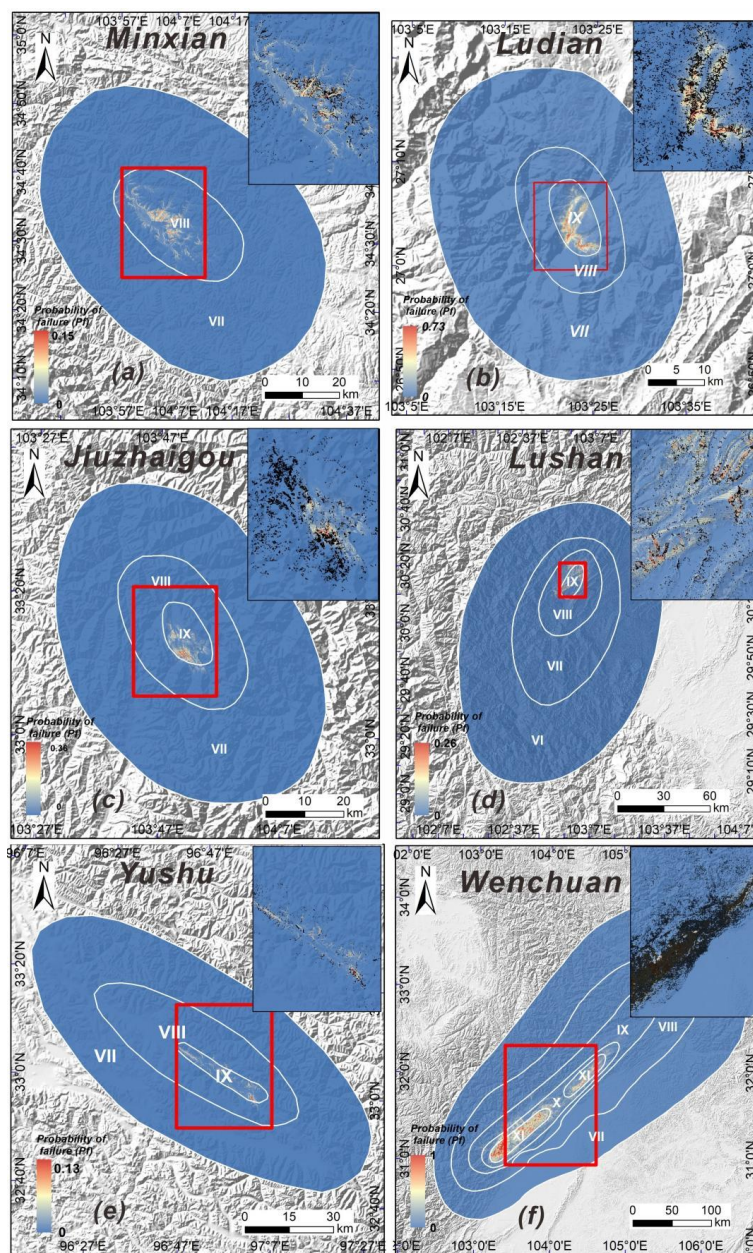
384 As mentioned in section 3.21, for the landslide hazard prediction of the second
385 and third stages, we train the evaluation model of these two stages using landslide



386 data from the meizoseismal area and the whole quake-affected area respectively. To
387 reduce the stochastic effects of data sampling, we calculate the LR model by randomly
388 selecting the training samples by considering the uncertainty of the samples ([Shao et](#)
389 [al., 2020b](#)). All the predicted models for 6 earthquake cases are performed 50 times,
390 yielding 50 predicted pictures of potential landslides in the study area for each event.

391 Fig.6 shows the mean predicted probability distribution of six events in the
392 second stage. The majority of the high-hazard-risk areas of six earthquakes are located
393 in high-intensity areas. For example, the high-hazard-risk areas of the Ludian
394 earthquake are concentrated in the meizoseismal area, which is essentially consistent
395 with the actual landslide distribution. However, in the southwest region where
396 landslides are well developed beyond the meizoseismal area with intensity VIII, the
397 landslide density is high, but the predict probability is quite low. Similar phenomena
398 have been observed in the Jiuzhaigou and Lushan earthquakes. The above
399 phenomenon is less obvious in other three earthquake events including the Minxian,
400 Wenchuan, and Yushu earthquakes. For instance, the seismogenic fault of the Yushu
401 earthquake is a left-lateral strike-slip fault, and thus the majority of the coseismic
402 landslides are basically distributed along both sides of the seismogenic fault. The high
403 hazard areas of the Yushu earthquake are distributed in the meizoseismal area on both
404 sides of the seismogenic fault, and these areas essentially correspond to the main
405 development areas of seismic landslides.

406 Based on the same method, we use all landslide data of the whole earthquake
407 affected area to calculate the prediction probability distribution map of the third stage.
408 Compared to the second stage, the predicted results in the third one are more
409 consistent with the actual landslide distribution. The majority of actual landslides are
410 basically distributed in areas with high hazard risk, indicating that the evaluation model
411 has high prediction ability at this stage. Particularly for the Ludian, Jiuzhaigou and
412 Lushan earthquakes, the assessment results can better predict the actual landslide
413 distribution in all earthquake affected areas.



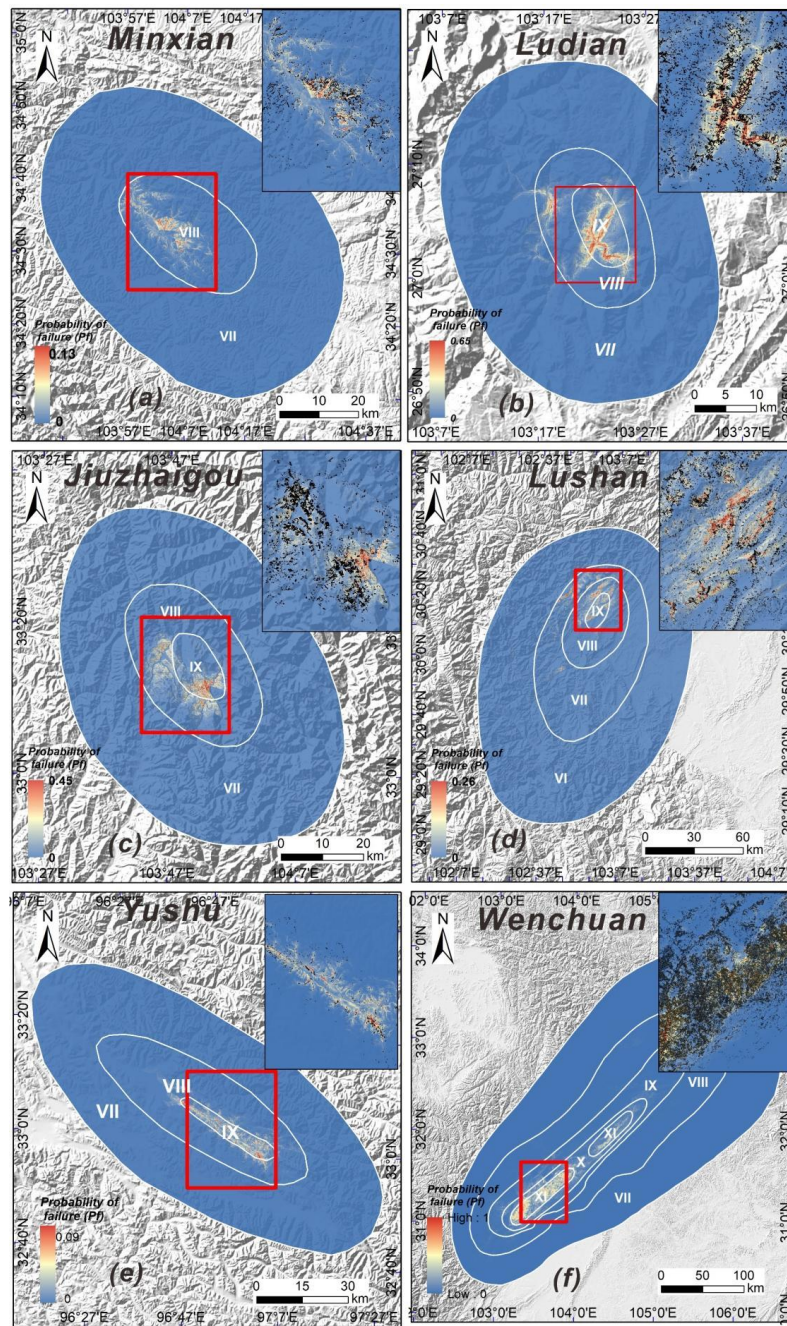
414

415 Fig.6 Maps showing predicted landslide probability distribution for six earthquake events in the
416 second stage; (a) the 2013 Mw 5.9 Minxian earthquake; (b) the 2014 Mw 6.6 Ludian earthquake;
417 (c) the 2017 Mw 6.5 Jiuzhaigou earthquake; (d) the 2013 Mw 6.6 Lushan earthquake; (e) the



418

2010 Mw 6.9 Yushu earthquake; (f) the 2008 Mw 7.9 Wenchuan earthquake;



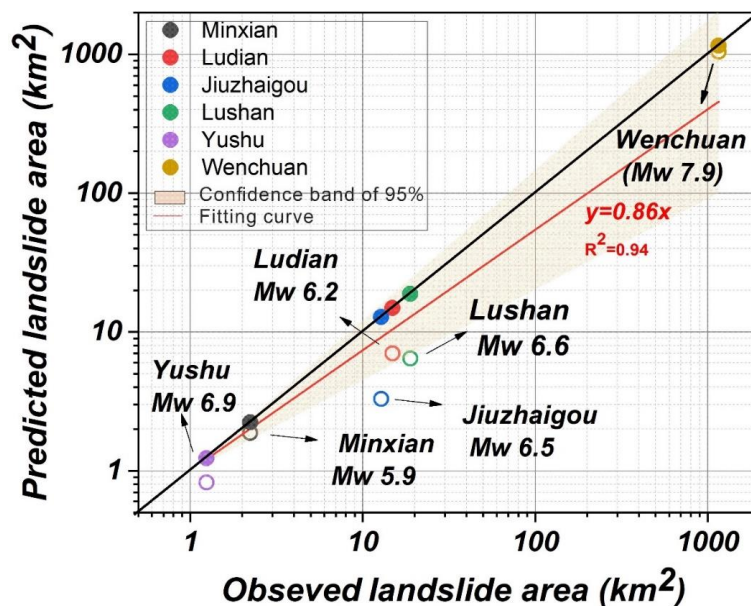
419

420 Fig.7 Maps showing predicted landslide probability distribution for six earthquake events in the



421 third stage; (a) the 2013 Mw 5.9 Minxian earthquake; (b) the 2014 Mw 6.6 Ludian earthquake; (c)
422 the 2017 Mw 6.5 Jiuzhaigou earthquake; (d) the 2013 Mw 6.6 Lushan earthquake; (e) the 2010
423 Mw 6.9 Yushu earthquake; (f) the 2008 Mw 7.9 Wenchuan earthquake;

424 Fig.8 shows the relationships between the observed landslide area (A_o) and the
425 predicted landslide area (A_p) for six earthquake events in the second and third stages.
426 The results show that whether in the second or third stage, A_p is in good agreement
427 with A_o . In the second stage, the slope of the fitting curves of the two stages are 0.86
428 and 1.01 respectively. In addition, we can observe that in the second stage, the A_p of
429 the six earthquakes are generally lower than the corresponding A_o , and the overall
430 error is between 9% and 74%. Among them, the prediction error of the Wenchuan
431 earthquake is the lowest (9%), and the error of the Jiuzhaigou earthquake is the
432 highest, reaching 74%. For the six cases in the third stage, A_p is basically consistent
433 with A_o , and the error range is about 1%, showing high performance of LR model in
434 this stage.



435

436 Fig.8 Relationships between the observed landslide area (A_o) and the predicted landslide

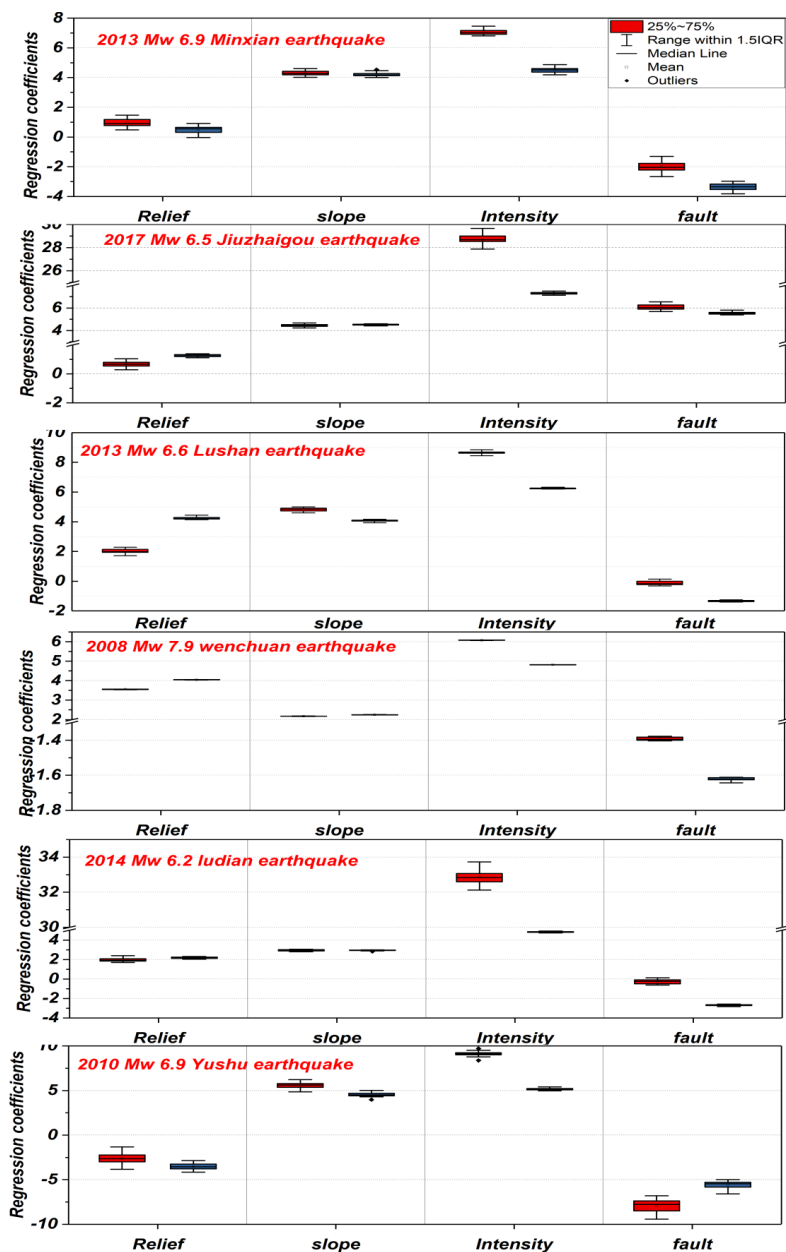


437 area (A_p) for six earthquake events in the second and third stages; The hollow and filled
438 circles represent the predicted landslide area for the second and third stages, respectively.

439 The red and black lines represent the fitting curves of the second and third stages,
440 respectively.

441 Fig.9 shows the distribution of regression coefficients of various influencing
442 factors in the second and third stages. For continuous variables, if the regression
443 coefficient is positive, with the increase of the independent variable, the probability
444 of landslide risk is larger ([Nowicki Jessee et al., 2018](#); [Shao et al., 2020a](#)). According to
445 the regression coefficient, we can explain the relationship between each influencing
446 factor and the corresponding landslide occurrence. We choose four independent
447 variables which have large impact on landslide occurrence: topographic relief, slope,
448 seismic intensity, and distance to seismogenic fault. The results show that regression
449 coefficient of seismic intensity is the largest in all seismic events, followed by slope
450 angle, indicating that the seismic factor and slope angle are the main factors
451 controlling the occurrence of seismic landslides. Furthermore, the distance to fault is
452 another important factor that controls the occurrence of seismic Landslides. The
453 regression coefficient of this variable is negative, implying that it has a negative effect
454 on the occurrence of seismic landslides (i.e., the farther away from the seismogenic
455 fault, the less likely the occurrence of seismic landslides). Furthermore, with the
456 exception of the 2010 Yushu earthquake, the regression coefficients of topographic
457 relief in the other five earthquake events are all positive, indicating that topographic
458 relief in other five earthquake events contributes positively to the occurrence of
459 seismic landslides.

460



461
462

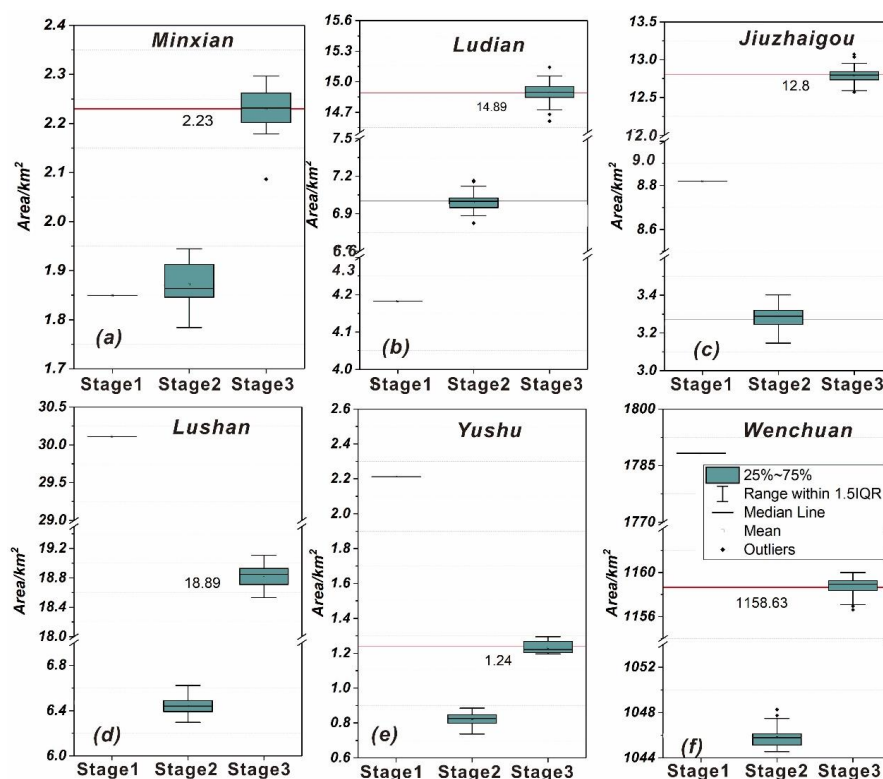
Fig.9 Regression coefficients of independent variables at different evaluation stages

463 4.3 Quantitative analysis

464 In order to quantitatively analyze the model results of the six earthquakes at
465 different stages, three indexes including the receiver operating characteristics (ROC)
466 curve, the confusion matrix and the predicted landslide area (A_p) are used to evaluate



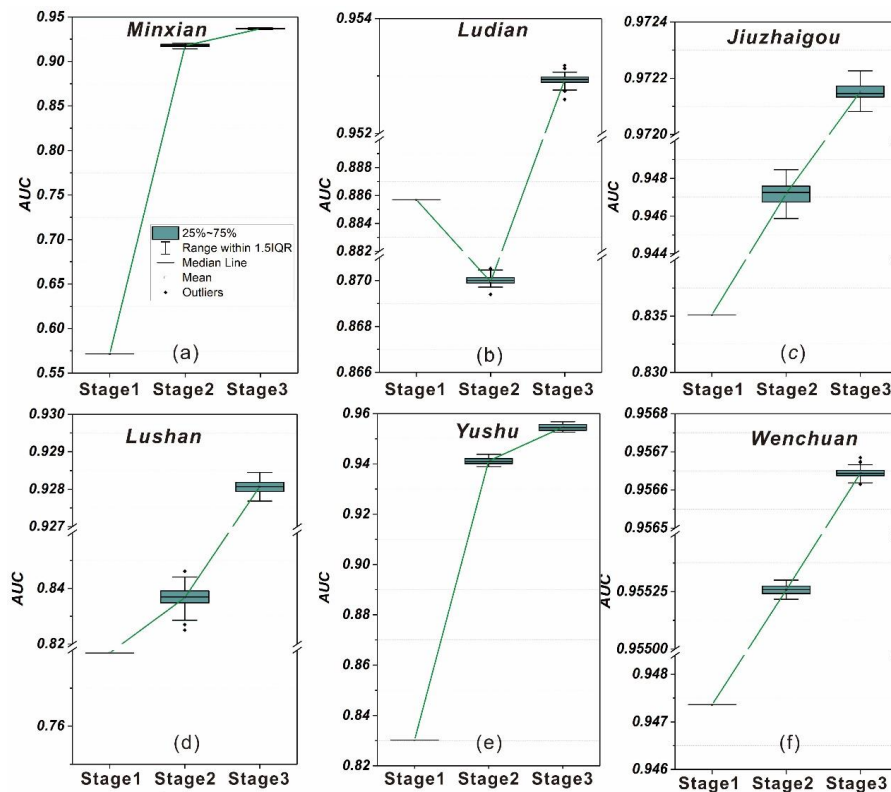
467 our model results. Fig.10 shows the predicted landslide area for six earthquake events
 468 in different stages. The results reveal that the A_p of the three events including the
 469 Minxian, Ludian, and Jiuzhaigou earthquakes in the first stage is much lower than the
 470 corresponding A_o , whereas the A_p of the Lushan, Yushu, and Wenchuan earthquakes
 471 is significantly greater. Furthermore, based on incomplete landslide data in the
 472 meizoseismal area, A_p is much smaller than A_o . However, when the prediction model
 473 based on complete landslide data is built, A_p is nearly identical to A_o .



474
 475 Fig.10 Predicted landslide area for six earthquake events in different evaluation stages. The
 476 horizontal line represents the total area of landslides triggered by this earthquake
 477 Fig.11 shows the distribution of AUC values for six earthquake events in different
 478 stages. The result show that aside from the Ludian earthquake, the prediction accuracy
 479 of the model outputs for other five earthquake events exhibits an upward trend. In the
 480 first stage, the AUC value of the modelling performance of the Wenchuan earthquake



481 is the highest, reaching 0.947, while the AUC value of the Minxian earthquake is the
482 lowest, only 0.57. Furthermore, the AUC values of other four earthquakes range from
483 0.8 to 0.85. In the second and third stages, we can observe that as landslide data
484 quality is continuously improved, the prediction ability of the model based on the
485 entire landslide database is gradually increased. Based on the entire landslide
486 database, the AUC value of six events exceeds 0.9, indicating a very high prediction
487 accuracy.

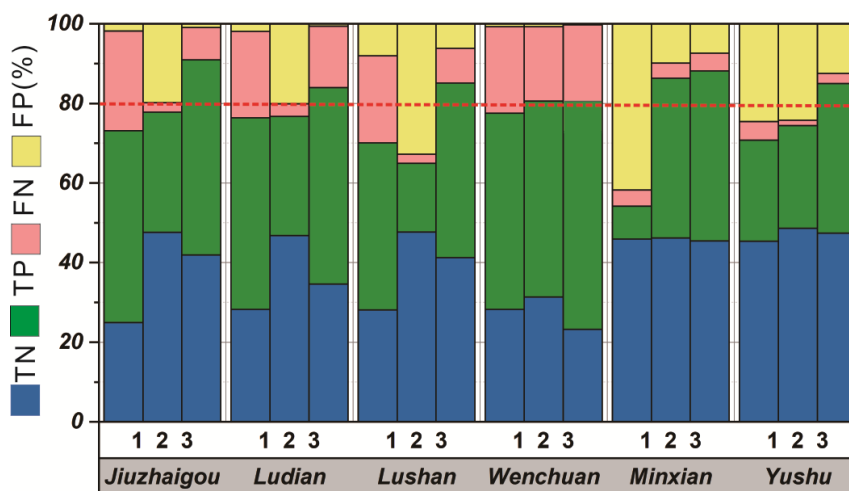


488
489 Fig.11 Distribution of AUC values for the six earthquake events in different evaluation stages.

490 Fig. 12 shows the calculated model accuracy using actual landslide data from the
491 six seismic events at different stages. The accuracy of the model fluctuates from 58%
492 to 78% at the first stage, indicating that the model's applicability in different seismic
493 events changes. In the second stage, with the exception of the Wenchuan earthquake,
494 the accuracy of other earthquake events is less than 80%. In the third stage, the model



495 accuracy of all seismic events exceeds 80%, with the Jiuzhaigou event reaching 91%.



496

497 Fig.12 Results of models validated by the six earthquake inventories. TN: True Negative; TP: True
498 Positive; FN: False Negative; FP: False Positive. The accuracy (ACC) of the models represented
499 graphically by the sum of the two lower bars.

500

501 5 Discussion

502 Time is of the essence in the emergency response stage I. Rapid evaluation of
503 earthquake-induced landslides can quickly determine the high-risk areas of coseismic
504 landslides and provide a basis for optimizing emergency deployment. Despite the fact
505 that the Newmark model is widely used in the emergency evaluation of earthquake-
506 induced landslides, this method is affected by input parameters and model
507 simplification, resulting in the problem of practicability in the emergency rescue
508 stages (Ma and Xu, 2019b). As a result, in recent years, the near real-time coseismic
509 landslide models based on global landslide data have been proposed and tested in
510 some earthquake cases. Allstadt et al. (2018) compare three global earthquake-
511 induced landslide models and use the 2016 Mw 7.8 Kaikoura, New Zealand,
512 earthquake to evaluate the performance of three models. The seismic landslide hazard
513 assessment map of this earthquake event is created by the above models and the



514 ShakeMap published by USGS, which demonstrate the remarkable potential of the
515 near real-time model in earthquake landslide emergency assessment. Similarly, [Xu et](#)
516 [al. \(2019\)](#) establish a new generation of Chinese earthquake-triggered landslide hazard
517 model based on 9 real earthquake-triggered landslide cases. We apply this model to
518 the six earthquake events in the Sichuan Yunnan region and the result shows that
519 although the prediction result based on this model is the landslide hazard estimate
520 with 100m resolution, the model can quickly determine the high-hazard-risk area after
521 the earthquake. Furthermore, with the exception of the Minxian earthquake, the
522 model shows strong prediction ability in other five events, and the AUC values are
523 greater than 0.8 (Fig.11). However, the AUC value of the Minxian event is only 0.57,
524 illustrating that the model is inapplicable in the Minxian region (Fig.11).

525 The main lithology of the landslides triggered by the earthquake in Minxian region
526 is Pleistocene loess, and thus the main landslide type is small- and medium-sized loess
527 landslide ([Xu et al., 2014a](#)). In contrast, the coseismic landslides triggered by other five
528 events are primarily rock landslides. Furthermore, the landform of the Minxian area is
529 typical loess landform with thick loess covering the hillside. The remaining five
530 earthquake zones are typical mountainous landforms with high altitudes and steep
531 slopes, and the rock joints are well developed due to the strong influence of tectonic
532 activity. Therefore, the Minxian earthquake has very different geological, topographic,
533 and geomorphic conditions, compared with other five earthquake events. Such
534 differences lead to the poor evaluation ability of the model for the Minxian earthquake.
535 Otherwise, the AUC value of the Wenchuan earthquake is the highest, reaching 0.947
536 (Fig.11). The Chinese earthquake-triggered landslide hazard model includes more than
537 300000 real landslide records, of which the landslide records of the Wenchuan
538 earthquake account for more than 60% of the total records. Because of the relative
539 large number of landslides triggered by the Wenchuan event, the global data set
540 remains dominated by this earthquake, the construction of the LR model is most
541 affected by the landslide samples of the Wenchuan events, which leads to the highest
542 applicability and accuracy of the model in the Wenchuan region. The same
543 phenomenon can also be found in previous studies ([Nowicki Jessee et al., 2018](#);



544 [Nowicki et al., 2014](#)).

545 Despite the fact that remote sensing and GIS technology have advanced
546 significantly in recent years, a considerable amount of post-earthquake images may
547 appear within a few hours or days after the earthquake. However, due to the broad
548 quake-affected area, cloud coverage, satellite scheduling and other factors, it is
549 difficult to acquire the post-quake optical imagery immediately ([Kargel et al., 2016](#);
550 [Roback et al., 2018](#)). Therefore, in the temporary resettlement stage II, we can only
551 obtain the images of the meizoseismal area, and carry out visual interpretation or
552 automatic identification of the seismic landslides in this area. [Robinson et al. \(2017\)](#)
553 use the coseismic landslide database of the 2016 Nepal earthquake to conduct the
554 rapid post-earthquake modelling of coseismic landslide. The evaluation results
555 obtained by randomly a small number of landslide samples are not much different
556 from those obtained by using the complete landslide database, indicating that
557 incomplete landslide samples can also be used to conduct seismic landslide hazard
558 assessment. Our findings also reveal that the AUC values of all seismic events in the
559 second stage are greater than 0.8, indicating that the prediction results based on
560 incomplete landslide data in the meizoseismal area can better predict the location of
561 the landslides in the entire earthquake area (Fig.11 and 12). Although the A_p
562 calculated by incomplete landslide data is slightly less than the A_o triggered by
563 earthquake events (Fig.10), on the whole, the prediction model has certain
564 applicability in the mid-term stage of the earthquake, which can better take into
565 account the timeliness and accuracy, in order to better serve the post resettlement of
566 earthquake stricken areas ([Ma et al., 2020](#)).

567 **6 Conclusion**

568 The aim of this study is to propose an improved three-stage spatial prediction
569 strategy and evaluate the applicability of this strategy in six earthquake events. The
570 results reveal that in the first stage, the AUC value of the modelling performance of
571 the Wenchuan earthquake is the highest, reaching 0.947, while the AUC value of the
572 Minxian earthquake is the lowest, only 0.57. In the second and third stages, we can



573 observe that as landslide data is continuously improved, the prediction ability of the
574 model based on the entire landslide database is gradually enhanced. Based on the
575 entire landslide database, the AUC values of six events exceed 0.9, indicating a very
576 high prediction accuracy. Furthermore, the A_p for the six earthquake events in
577 different evaluation stages shows that based on incomplete landslide data in the
578 meizoseismal area, A_p is much smaller than A_o . Nevertheless, when the prediction
579 model based on complete landslide data is built, A_p is nearly identical to A_o . Overall,
580 the prediction results in the first stage can meet the requirements of emergency
581 rescue with quickly obtaining the overall predicted information of the possible
582 coseismic landslide locations in the quake-affected area. With the improvement of the
583 coseismic landslide data in the second and third stages, the accuracy of the prediction
584 results can be more accurate, and thus it can meet the requirement of temporary
585 restoration and later reconstruction. This improved three-stage spatial prediction
586 strategy has preferable practicability for regional landslide disaster prevention and
587 mitigation of the major earthquakes in the Sichuan and Yunnan regions.

588 **Author contributions**

589 C.X. conceptualized the work, designed the overall methodology. X.S. wrote the
590 codes of Mat.LShazard and original draft of the paper. S.M. designed the framework
591 of this research, processed the relevant data and performed the overall Mat.LShazard
592 code validation. S.M. and C.X. contributed to the review, editing, and writing of the
593 paper.

594 **Code availability**

595 Mat.LShazard V1.0 is composed of three modules including Data input, model
596 training, and model validation coded as separate matlab script files and can be
597 executed under WindowsOS with the version of MATLAB 2016 or higher. Mat.LShazard
598 V1.0 is free software, and the codes are all public.

599 The source codes are available for download at
600 [thehttps://zenodo.org/record/7074082#.YyAxMqRBxPY](https://zenodo.org/record/7074082#.YyAxMqRBxPY).



601

602 **Data availability**

603 Data used in this analysis include mapped landslide inventories of the 2008 Mw
604 7.9 Wenchuan earthquake (Xu et al., 2014b), the 2014 Mw 6.6 Ludian earthquake (Wu
605 et al., 2020), the 2013 Mw 6.6 Lushan earthquake (Xu et al., 2015), the 2017 Mw 6.5
606 Jiuzhaigou earthquake (Tian et al., 2019), the 2013 Mw 5.9 Minxian earthquake (Tian
607 et al., 2016), the 2010 Mw 6.9 Yushu earthquake (Xu and Xu, 2014). A subset of these
608 landslide inventories is publicly available in an open access data repository from
609 <https://www.sciencebase.gov/catalog/item/586d824ce4b0f5ce109fc9a6>. The
610 elevation data is from 30m resolution SRTM DEM (Jarvis et al., 2008). The distribution
611 of seismic intensity for every seismic event is provided by China Earthquake Networks
612 Center (<https://www.cenc.ac.cn/cenc/zgdztw/index.html>). Lithology data are from
613 China Geological Survey (<http://dcc.cgs.gov.cn/>).

614 **Acknowledgments**

615 This study was supported by the National Institute of Natural Hazards, Ministry
616 of Emergency Management of China (ZDJ2021-14) and the Lhasa National Geophysical
617 Observation and Research Station (NORSLS20-07).

618

619 **References**

- 620 Allstadt K E, Jibson R W, Thompson E M et al., 2018. Improving Near-Real-Time Coseismic Landslide
621 Models: Lessons Learned from the 2016 Kaikōura, New Zealand, Earthquake. *Bulletin of the*
622 *Seismological Society of America*, 108, 1649-1664.
- 623 Bai S B, Lu P, Wang J, 2015. Landslide susceptibility assessment of the Youfang Catchment using logistic
624 regression. *Journal of Mountain Science*, 816-827.
- 625 Bragagnolo L, da Silva R V, Grzybowski J M V, 2020. Landslide susceptibility mapping with r.landslide: A
626 free open-source GIS-integrated tool based on Artificial Neural Networks. *Environmental*
627 *Modelling & Software*, 123, 104565.
- 628 Brenning A, 2005. Spatial prediction models for landslide hazards: review, comparison and evaluation.
629 *Natural Hazards & Earth System Sciences*, 5, 853-862.
- 630 Broeckx J, Vanmaercke M, Duchateau R et al., 2018. A data-based landslide susceptibility map of Africa.
631 *Earth-Science Reviews*, 185, 102-121.
- 632 Cao J, Zhang Z, Wang C et al., 2019. Susceptibility assessment of landslides triggered by earthquakes in



-
- 633 the Western Sichuan Plateau. *CATENA*, 175, 63-76.
- 634 Chen L, Wang H, Ran Y et al., 2010. The MS7.1 Yushu earthquake surface rupture and large historical
635 earthquakes on the Garzê-Yushu Fault. *Chinese Science Bulletin*, 55, 3504-3509.
- 636 Cheng J, Xu X, Chen G, 2020. A new prediction model of seismic hazard for the Sichuan-Yunnan region
637 based on the occurrence rate of large earthquakes. *Journal of Geophysics*, 63.
- 638 Cui P, Zhu Y-y, Han Y-s et al., 2009. The 12 May Wenchuan earthquake-induced landslide lakes:
639 distribution and preliminary risk evaluation. *Landslides*, 6, 209-223.
- 640 Dai F, Lee C F, Li J et al., 2001. Assessment of landslide susceptibility on the natural terrain of Lantau
641 Island, Hong Kong. *Environmental Geology*, 40, 381-391.
- 642 Dai F C, Lee C F, 2002. Landslide characteristics and slope instability modeling using GIS, Lantau Island,
643 Hong Kong. *Geomorphology*, 42, 213-228.
- 644 Demir G, Aytekin M, Akgün A et al., 2013. A comparison of landslide susceptibility mapping of the
645 eastern part of the North Anatolian Fault Zone (Turkey) by likelihood-frequency ratio and
646 analytic hierarchy process methods. *Natural Hazards*, 65, 1481-1506.
- 647 Dreyfus D K, Rathje E M, Jibson R W, 2013. The influence of different simplified sliding-block models and
648 input parameters on regional predictions of seismic landslides triggered by the Northridge
649 earthquake. *Engineering Geology*, 163, 41-54.
- 650 Ercanoglu M, Temiz F A, 2011. Application of logistic regression and fuzzy operators to landslide
651 susceptibility assessment in Azdavay (Kastamonu, Turkey). *Environmental Earth Sciences*, 64,
652 949-964.
- 653 Fawcett T, 2006. An introduction to ROC analysis. *Pattern Recognition Letters*, 27, 861-874.
- 654 Fick S E, Hijmans R J, 2017. WorldClim 2: new 1-km spatial resolution climate surfaces for global land
655 areas. *International Journal of Climatology*, 37, 4302-4315.
- 656 Guzzetti F, Paola R, Cardinali M et al., 2005. Probabilistic landslide hazard assessment at the basin scale.
657 *Geomorphology*, 72, 272-299.
- 658 He Q, Wang M, Liu K, 2021. Rapidly assessing earthquake-induced landslide susceptibility on a global
659 scale using random forest. *Geomorphology*, 391, 107889.
- 660 Huang R, Fan X, 2013. The landslide story. *Nature Geoscience*, 6, 325-326.
- 661 Jarvis A, Reuter H, Nelson A et al., 2008. Hole-filled seamless SRTM data v4. International Centre for
662 Tropical Agriculture (CIAT).
- 663 Jiang W, Zhang J, Tian T et al., 2012. Crustal structure of Chuan-Dian region derived from gravity data
664 and its tectonic implications. *Physics of the Earth and Planetary Interiors*, 212-213, 76-87.
- 665 Jibson R W, Harp E L, Michael J A, 2000. A method for producing digital probabilistic seismic landslide
666 hazard maps: An example from the Los Angeles, California, area. *Engineering Geology*, 58, 271-
667 289.
- 668 Kargel J S, Leonard G J, Shugar D H et al., 2016. Geomorphic and geologic controls of geohazards induced
669 by Nepal's 2015 Gorkha earthquake. *Science*, 351, aac8353.
- 670 Kritikos T, Robinson T R, Davies T R H, 2015. Regional coseismic landslide hazard assessment without
671 historical landslide inventories: A new approach. *Journal of Geophysical Research Earth Surface*,
672 120, 711-729.
- 673 Lan H, Tian N, Li L et al., 2022. Poverty control policy may affect the transition of geological disaster risk
674 in China. *Humanities and Social Sciences Communications*, 9, 80.
- 675 Lari S, Frattini P, Crosta G B, 2014. A probabilistic approach for landslide hazard analysis. *Engineering
676 Geology*, 182, 3-14.



-
- 677 Lin L, Lin Q, Wang Y, 2017. Landslide susceptibility mapping on a global scale using the method of logistic
678 regression. *Nat. Hazards Earth Syst. Sci.*, 17, 1411-1424.
- 679 Liu J, Wang T, Shi J et al., 2017. Emergency Rapid Assessment of Landslides Induced by the Jiuzhaigou
680 M s 7.0 earthquake, Sichuan, China. *Journal of Geomechanics*, 23, 639-645.
- 681 Ma S, Xu C, 2019a. Applicability of Two Newmark Models in the Assessment of Coseismic Landslide
682 Hazard and Estimation of Slope-Failure Probability: An Example of the 2008 Wenchuan Mw 7.9
683 Earthquake Affected Area. *Journal of Earth Science*, 30, 1020-1030.
- 684 Ma S, Xu C, Shao X, 2020. Spatial prediction strategy for landslides triggered by large earthquakes
685 oriented to emergency response, mid-term resettlement and later reconstruction.
686 *International Journal of Disaster Risk Reduction*, 43, 101362.
- 687 Ma S Y, Xu C, 2019b. Assessment of co-seismic landslide hazard using the Newmark model and statistical
688 analyses: a case study of the 2013 Lushan, China, Mw6.6 earthquake. *Natural Hazards*, 96, 389-
689 412.
- 690 Massey C, Townsend D, Rathje E et al., 2018. Landslides Triggered by the 14 November 2016 Mw 7.8
691 Kaikōura Earthquake, New Zealand. *Bulletin of the Seismological Society of America*, 108, 1630-
692 1648.
- 693 Merghadi A, Yunus A P, Dou J et al., 2020. Machine learning methods for landslide susceptibility studies:
694 A comparative overview of algorithm performance. *Earth-Science Reviews*, 207, 103225.
- 695 Nowicki Jesse M A, Hamburger M W, Allstadt K et al., 2018. A global empirical model for near-real-time
696 assessment of seismically induced landslides. *Journal of Geophysical Research: Earth Surface*,
697 123, 1835-1859.
- 698 Nowicki M A, Wald D J, Hamburger M W et al., 2014. Development of a globally applicable model for
699 near real-time prediction of seismically induced landslides. *Engineering Geology*, 173, 54-65.
- 700 Osna T, Sezer E A, Akgun A, 2014. GeoFIS: An integrated tool for the assessment of landslide
701 susceptibility. *Computers & Geosciences*, 66, 20-30.
- 702 Polat A, 2021. An innovative, fast method for landslide susceptibility mapping using GIS-based LSAT
703 toolbox. *Environmental Earth Sciences*, 80, 217.
- 704 Pradhan B, Saro L, 2010. Landslide susceptibility assessment and factor effect analysis: backpropagation
705 artificial neural networks and their comparison with frequency ratio and bivariate logistic
706 regression modelling. *Environmental Modelling & Software*, 25, 747-759.
- 707 Reichenbach P, Rossi M, Malamud B D et al., 2018. A review of statistically-based landslide susceptibility
708 models. *Earth-Science Reviews*, 180, 60-91.
- 709 Ren J, Xu X, Lv Y et al., 2022. Late Quaternary slip rate of the northern Lancangjiang fault zone in eastern
710 Tibet: Seismic hazards for the Sichuan-Tibet Railway and regional tectonic implications.
711 *Engineering Geology*, 106748.
- 712 Roback K, Clark M K, West A J et al., 2018. The size, distribution, and mobility of landslides caused by
713 the 2015 Mw7.8 Gorkha earthquake, Nepal. *Geomorphology*, 301, 121-138.
- 714 Robinson T R, Rosser N J, Densmore A L et al., 2017. Rapid post-earthquake modelling of coseismic
715 landslide intensity and distribution for emergency response decision support. *Nat. Hazards
716 Earth Syst. Sci.*, 17, 1521-1540.
- 717 Rossi M, Reichenbach P, 2016. LAND-SE: a software for statistically based landslide susceptibility
718 zonation, version 1.0. *Geoscientific Model Development*, 9, 3533-3543.
- 719 Shao X, Ma S, Xu C et al., 2020a. Effects of raster resolution on real probability of landslides. *Remote
720 Sensing Applications: Society and Environment*, 19, 100364.



-
- 721 Shao X, Ma S, Xu C et al., 2020b. Effects of sampling intensity and non-slide/slide sample ratio on the
722 occurrence probability of coseismic landslides. *Geomorphology*, 363, 107222.
- 723 Shao X, Xu C, 2022. Earthquake-induced landslides susceptibility assessment: A review of the state-of-
724 the-art. *Natural Hazards Research*.
- 725 Sun J, Yue H, Shen Z et al., 2018. The 2017 Jiuzhaigou Earthquake: A Complicated Event Occurred in a
726 Young Fault System. *Geophysical Research Letters*, 45, 2230-2240.
- 727 Swets J A, 1988. Measuring the accuracy of diagnostic systems. *Science*, 240, 1285-1293.
- 728 Tanyas H, Rossi M, Alvioli M et al., 2019. A global slope unit-based method for the near real-time
729 prediction of earthquake-induced landslides. *Geomorphology*, 327, 126-146.
- 730 Tapponnier P, Zhiqin X, Roger F et al., 2001. Oblique stepwise rise and growth of the Tibet plateau.
731 *Science*, 294, 1671-1677.
- 732 Tateishi R, 2010. Production of global land cover data-GLCNMO. *T. J. Digital Earth*, 4, 22-49.
- 733 Tian Y, Owen L A, Xu C et al., 2020. Landslide development within 3 years after the 2015 Mw 7.8 Gorkha
734 earthquake, Nepal. *Landslides*, 17, 1251-1267.
- 735 Tian Y, Xu C, Ma S et al., 2019. Inventory and Spatial Distribution of Landslides Triggered by the 8th
736 August 2017 MW 6.5 Jiuzhaigou Earthquake, China. *Journal of Earth Science*, 30, 206-217.
- 737 Tian Y, Xu C, Xu X et al., 2016. Detailed inventory mapping and spatial analyses to landslides induced by
738 the 2013 Ms 6.6 Minxian earthquake of China. *Journal of Earth Science*, 27, 1016-1026.
- 739 Tolles J, Meurer W J, 2016. Logistic Regression: Relating Patient Characteristics to Outcomes. *JAMA*, 316,
740 533-534.
- 741 Torizin J, Schüßler N, Fuchs M, 2022. Landslide Susceptibility Assessment Tools v1.0.0b – Project
742 Manager Suite: a new modular toolkit for landslide susceptibility assessment. *Geoscientific
743 Model Development*, 15, 2791-2812.
- 744 Umar Z, Pradhan B, Ahmad A et al., 2014. Earthquake induced landslide susceptibility mapping using an
745 integrated ensemble frequency ratio and logistic regression models in West Sumatera Province,
746 Indonesia. *Catena*, 118, 124-135.
- 747 Wang Y, Song C, Lin Q et al., 2016. Occurrence probability assessment of earthquake-triggered landslides
748 with Newmark displacement values and logistic regression: The Wenchuan earthquake, China.
749 *Geomorphology*, 258, 108-119.
- 750 Wu W, Xu C, Wang X et al., 2020. Landslides Triggered by the 3 August 2014 Ludian (China) Mw 6.2
751 Earthquake: An Updated Inventory and Analysis of Their Spatial Distribution. *Journal of Earth
752 Science*, 31, 853-866.
- 753 Xu C, Dai F, Xu X et al., 2012. GIS-based support vector machine modeling of earthquake-triggered
754 landslide susceptibility in the Jianjiang River watershed, China. *Geomorphology*, 145-146, 70-
755 80.
- 756 Xu C, Xu X, 2014. Statistical analysis of landslides caused by the Mw 6.9 Yushu, China, earthquake of
757 April 14, 2010. *Natural Hazards*, 72, 871-893.
- 758 Xu C, Xu X, Shyu J B H, 2015. Database and spatial distribution of landslides triggered by the Lushan,
759 China Mw 6.6 earthquake of 20 April 2013. *Geomorphology*, 248, 77-92.
- 760 Xu C, Xu X, Shyu J B H et al., 2014a. Landslides triggered by the 22 July 2013 Minxian–Zhangxian, China,
761 Mw 5.9 earthquake: Inventory compiling and spatial distribution analysis. *Journal of Asian
762 Earth Sciences*, 92, 125-142.
- 763 Xu C, Xu X, Yao X et al., 2014b. Three (nearly) complete inventories of landslides triggered by the May
764 12, 2008 Wenchuan Mw 7.9 earthquake of China and their spatial distribution statistical



-
- 765 analysis. *Landslides*, 11, 441-461.
- 766 Xu C, Xu X, Zheng W et al., 2013. landslides triggered by the April 20, 2013 Lushan, Sichuan province M_s
767 7.0 strong earthquake of China. *Seismological geology*, 35, 641-660.
- 768 Xu C, Xu X, Zhou B et al., 2019. Probability of coseismic landslides: A new generation of earthquake-
769 triggered landslide hazard model. *Journal of Engineering Geology*, 27, 1122.
- 770 Xu X, Han Z, Yang X, 2016. Seismotectonic map in China and its adjacent regions. Seismological Press,
771 Beijing.
- 772 Xu X, Zhang P, Wen X et al., 2005. Features of active tectonics and recurrence behaviors of strong
773 earthquakes in the western Sichuan province and its adjacent regions. *Seismology and
774 geology*, 27, 446.
- 775 Xu X W, Wen X Z, Yu G H et al., 2009. Coseismic reverse- and oblique-slip surface faulting generated by
776 the 2008 Mw 7.9 Wenchuan earthquake, China. *Geology*, 37, 515-518.
- 777 Yao X, Tham L G, Dai F C, 2008. Landslide susceptibility mapping based on Support Vector Machine: A
778 case study on natural slopes of Hong Kong, China. *Geomorphology*, 101, 572-582.
- 779 Zhang P, Deng Q, Zhang G et al., 2003. Active tectonic blocks and strong earthquakes in the continent
780 of China. *Science in China Series D: Earth Sciences*, 46, 13-24.
- 781 Zhao B, Zhao X, Zeng L et al., 2021. The mechanisms of complex morphological features of a prehistorical
782 landslide on the eastern margin of the Qinghai-Tibetan Plateau. *Bulletin of Engineering
783 Geology and the Environment*, 80, 3423-3437.
- 784 Zheng W, Yuan D, He W et al., 2013. Geometric pattern and active tectonics in Southeastern Gansu
785 province: Discussion on seismogenic mechanism of the Minxian-Zhangxian M(S)6. 6
786 earthquake on July 22, 2013. *Chinese Journal of Geophysics*, 56, 4058-4071.
- 787 Zhuang J, Peng J, Zhu X et al., 2019. Scenario-Based Risk Assessment of Earthquake Disaster Using Slope
788 Displacement, PGA, and Population Density in the Guyuan Region, China. *ISPRS International
789 Journal of Geo-Information*, 8, 85.
- 790